

Hybrid Transmission Line for ECRH in the Helically Symmetric Experiment

J. W. Radder · K. M. Likin · F. S. B. Anderson ·
D. T. Anderson

Received: 19 November 2007 / Accepted: 24 January 2008 /
Published online: 29 February 2008
© Springer Science + Business Media, LLC 2008

Abstract The HSX oversized, mode-converting ECRH transmission line has been upgraded to a hybrid system to increase launched microwave power and reduce electrical arcing. Filtering of high-order, spurious modes ensures efficient coupling to a Gaussian beam for optimal electron heating. A Vlasov mode converter and two phase-correcting ellipsoidal mirrors convert the TE_{02} gyrotron output mode to a symmetric, linearly polarized, microwave beam. A swappable twist reflector plate rotates beam polarization for 2nd-harmonic X-mode or fundamental O-mode ECRH. Long distances are traversed by coupling the beam to a dual-mode ($TE_{11}+TM_{11}$), smooth, circular cross-section waveguide. This system has been successfully tested without arcing for 50 ms pulses and over 100 kW of launched power. Analysis of the microwave beam for 50 kW, 2 ms microwave pulses reveals agreement with predicted beam shapes at two beam locations. The new system has also demonstrated increased plasma stored energy for ECRH plasmas with equal launched power.

Keywords Electron cyclotron heating · Microwave transmission lines · Stellarators · Quasioptics

1 Introduction

The Helically Symmetric eXperiment (HSX) is a quasihelically symmetric (QHS) stellarator operating at the University of Wisconsin-Madison [1, 2]. HSX is a medium-sized stellarator ($R_0=1.2$ m, $a_r=0.15$ m) with 48 shaped modular coils and 48 planar auxiliary coils arranged in four field periods. The magnitude of the HSX magnetic field is dominated by a helical spectral component to produce the quasihelically symmetric configuration

J. W. Radder · K. M. Likin · F. S. B. Anderson · D. T. Anderson
HSX Plasma Laboratory, University of Wisconsin-Madison, Madison, WI 53706, USA

J. W. Radder (✉)
Electrical and Computer Engineering, University of Wisconsin-Madison,
1415 Engineering Drive, Madison, WI 53715, USA
e-mail: jradder@cae.wisc.edu

characterized by a helical magnetic axis with low toroidal curvature. The quasisymmetry can be broken by energizing the planar auxiliary coils to create conventional stellarator magnetic configurations.

Plasma breakdown and heating in HSX are accomplished via electron cyclotron resonance heating (ECRH) with a single 28 GHz gyrotron microwave source [3]. The gyrotron tube was manufactured by Varian (now CPI, Inc.) and is rated for maximum, pulsed operations of 200 kW, 75 ms with a TE₀₂ dominant output mode [4, 5]. TE₀₂-to-HE₁₁ mode conversion was previously accomplished with an oversized, mode-converting waveguide system. The maximum heating power of this system was limited to 50 kW by waveguide arcing. The oversized waveguide was replaced with a hybrid system in Spring 2006. This new line has been successfully tested for launched power values up to 100 kW in 0.5 Tesla, 2nd harmonic X-mode and 1.0 Tesla, fundamental O-mode ECRH.

2 Transmission line design

Design of the hybrid transmission line was reduced to five independent design problems: a quasioptical TE₀₂-to-TEM₀₀ mode converter, a matching unit, a polarizer, a dual-mode (TE₁₁+TM₁₁) waveguide, and a quasioptical switch, as shown in Figs. 1, 2 and 3. Mirrors were designed using quasioptical and passive high-power microwave component design techniques [6, 7]. All reflecting surfaces were machined from type 6061 aluminum to handle high thermal loads. Machining accuracies and surface finish specifications of modern CNC machining are adequate for three-dimensional phase-correcting mirrors operating at 28 GHz. A summary of mirror shapes is provided in Table 1.

The quasioptical mirrors were aligned with respect to an aluminum backplane to reduce the quasioptical system design to a two dimensional problem and to simplify mirror alignment. Reference detents were machined into the top and back surfaces of the mirrors as well as into the aluminum backplane. The detents were used as reference points to allow accurate mirror alignment with respect to the backplane with a coordinate measurement machine (CMM). The positions of the mirror reference points were within 0.08 mm of the original CAD drawings, and the mirror alignment was successfully completed in a single iteration.

2.1 TE₀₂-to-TEM₀₀ mode converter, matching unit, and polarizer

A Vlasov mode converter transforms the dominant TE₀₂ gyrotron output mode to an astigmatic Gaussian microwave beam, which approaches a free space TEM₀₀ mode plane wave in the far field. Conversion of cylindrical caustics to a plane wave is performed in the context of geometrical optics. Given a waveguide with radius, *a*, a given TE_{*m**n*} or TM_{*m**n*} mode is characterized by a caustic radius, *r_c*, bounce angle, *θ_B*, and bounce length, *L_B* [8]:

$$\theta_B = \arcsin(\kappa_{mn}/k) \tag{1}$$

$$r_c = m/\kappa_{mn} \tag{2}$$

$$L_B = 2\sqrt{a^2 - r_c^2} \cot \theta_B \tag{3}$$

$$\alpha = \arccos(r_c/a) \tag{4}$$

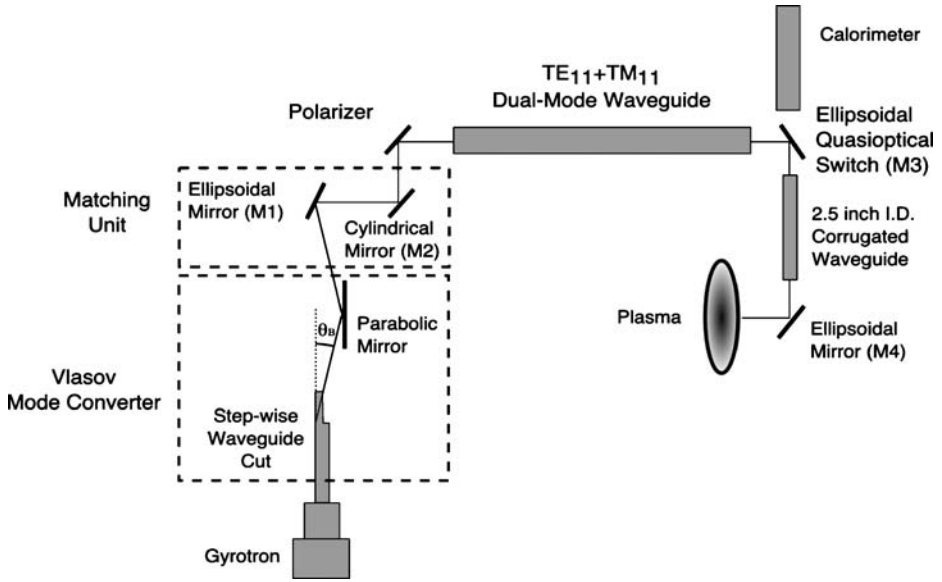


Fig. 1 Hybrid transmission line for plasma heating in the HSX Stellarator.

$$\kappa_{mn} = \begin{cases} \chi_{mn}/a & (\text{TM}_{mn} \text{ modes}) \\ \chi'_{mn}/a & (\text{TE}_{mn} \text{ modes}) \end{cases} \quad (5)$$

where k is the free space wave number and χ_{mn} and χ'_{mn} are the n th zeros of $J_m(x)$ and $J'_m(x)$, the Bessel function of the first kind and its derivative with respect to its argument, respectively. The TE_{02} mode is characterized by $\theta_B=22.1^\circ$, $r_c=0$, and $L_B=15.63$ cm for a waveguide with $a=3.175$ cm and a system frequency of 28 GHz.

The Vlasov converter for the TE_{02} mode consists of a step-wise waveguide cut and a mirror with a parabolic cross-section, as shown in Fig. 4. In order to completely radiate all power from symmetric ($m=0$) modes through the aperture formed by the step-wise cut, the

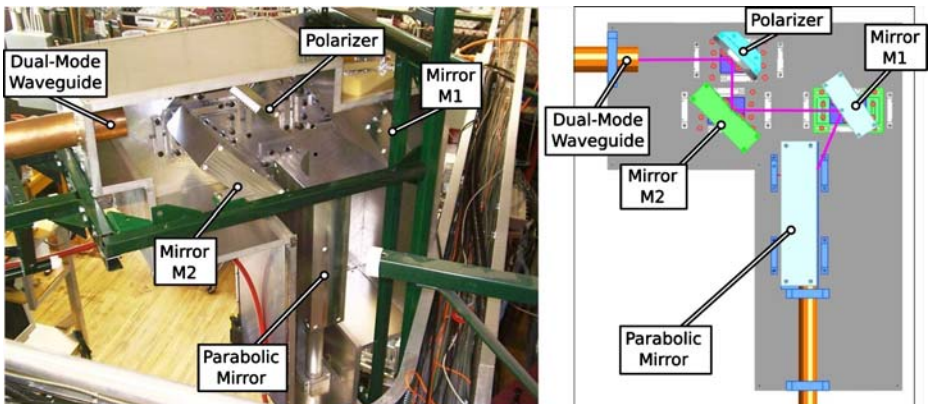
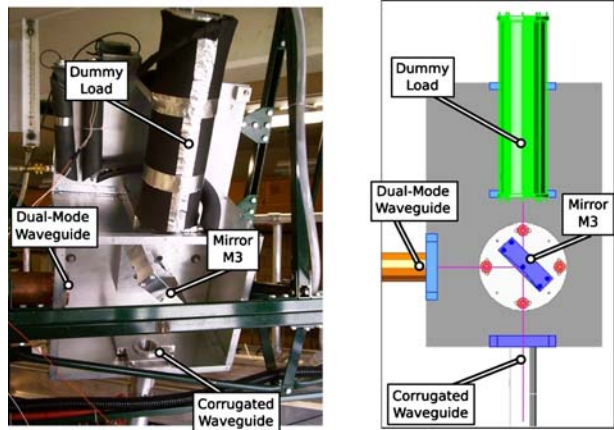


Fig. 2 TE_{02} -to- TEM_{00} mode converter photo (left) and CAD rendering (right).

Fig. 3 Quasioptical switch photo (left) and CAD rendering (right).



aperture length must be at least L_B and the angle formed by the aperture, α , must be at least 180° . The focal distance, F , is chosen to be 6.1 cm to prevent shadowing of the beam by the waveguide.

Vlasov converter efficiency is the product of the normalized power coupling coefficients calculated within and perpendicular to the plane of propagation. The electric field of a normalized Gaussian beam in Cartesian coordinates is

$$E(x, y, z) = \left(\frac{2}{\pi w_x w_y} \right)^{\frac{1}{2}} \exp \left(-\frac{x^2}{w_x^2} - \frac{y^2}{w_y^2} - jkz - \frac{j\pi x^2}{\lambda R_x} - \frac{j\pi y^2}{\lambda R_y} + j\phi \right), \quad (6)$$

where x and y are orthogonal to z , the direction of propagation. R_x and R_y are the curvature radii of the beam phase front, $w_x(z)$ and $w_y(z)$ are the beam radius, k is the free space wave number, λ is the wavelength, and ϕ_0 is an arbitrary phase. Equation 6 can be separated into a product of one dimensional field distributions,

$$E(x, y, z) = E_{ax}(x, z)E_{ay}(y, z) \exp \left(-\frac{j\pi x^2}{\lambda R_x} - \frac{j\pi y^2}{\lambda R_y} - jkz + j\phi_0 \right), \quad (7)$$

where

$$E_{ax}(x) = \left(\frac{2}{\pi w_x^2} \right)^{\frac{1}{4}} \exp \left(\frac{-x^2}{w_x^2} \right), \quad (8)$$

Table 1 Metallic mirror parameters. All values are given in millimeters.

Mirror	Curvature radius (\perp)	Curvature radius (\parallel)	Mirror size (\perp)	Mirror size (\parallel)
M1	1823.2	3975.3	386.1	275.4
M2	–	2050.6	225.1	321.7
M3	284.2	568.1	143.4	292.4
M4	232.5	464.7	142.7	248.4

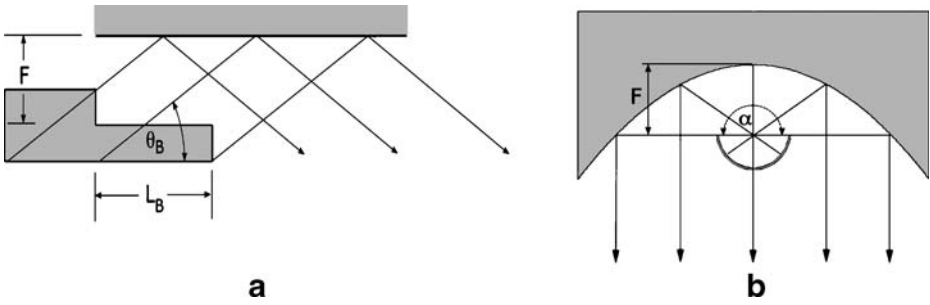


Fig. 4 Vlasov converter: (a) side view (b) end view.

$$E_{ay}(y) = \left(\frac{2}{\pi w_y^2} \right)^{\frac{1}{4}} \exp \left(\frac{-y^2}{w_y^2} \right). \tag{9}$$

The normalized one-dimensional field coupling coefficient is

$$c_{ab}^{1u} = \frac{\int E_{au}^*(u) f_b(u) du}{[\int E_{au}^*(u) E_{au}(u) du]^{0.5} [\int f_b^*(u) f_b(u) du]^{0.5}}, \tag{10}$$

where \$u\$ is either \$x\$ or \$y\$. \$E_{au}(u)\$ is the Gaussian beam electric field magnitude given by Eqs. 8 and 9, and \$f_b(u)\$ is an arbitrary electric field magnitude. The power coupling coefficient, \$K_{ab}\$, is the product of the squares of magnitudes of the one-dimensional field coefficients such that

$$K_{ab} = |c_{ab}^{1x}|^2 \cdot |c_{ab}^{1y}|^2, \tag{11}$$

where \$x\$ is oriented within and \$y\$ is perpendicular to the plane of beam propagation, along the beam path.

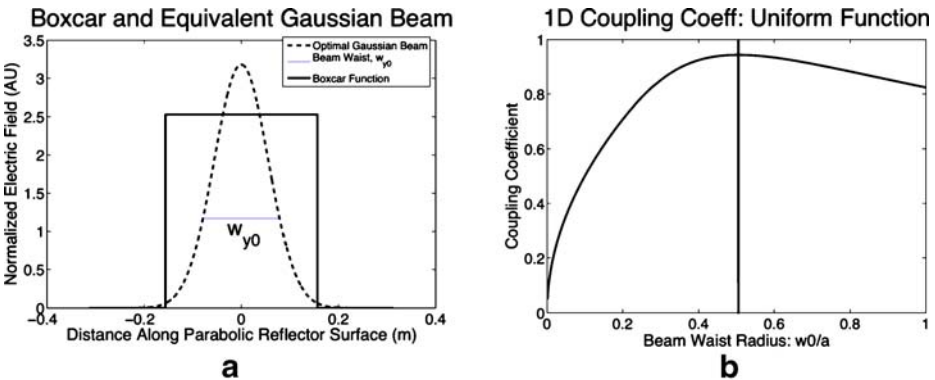


Fig. 5 (a) Boxcar function (b) normalized coupling coefficient.

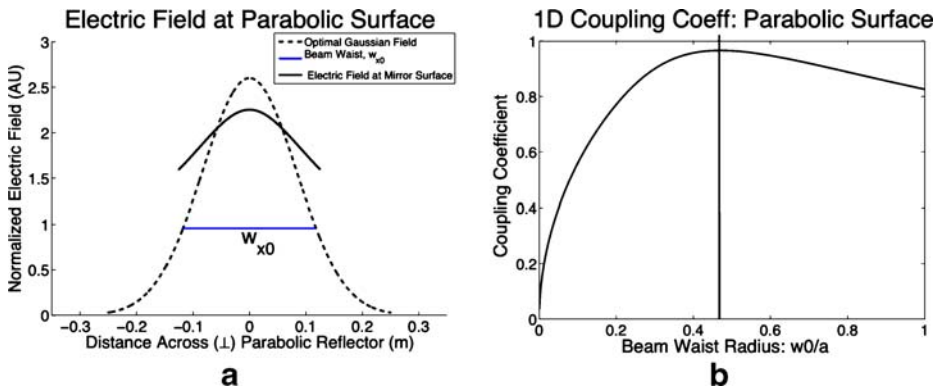


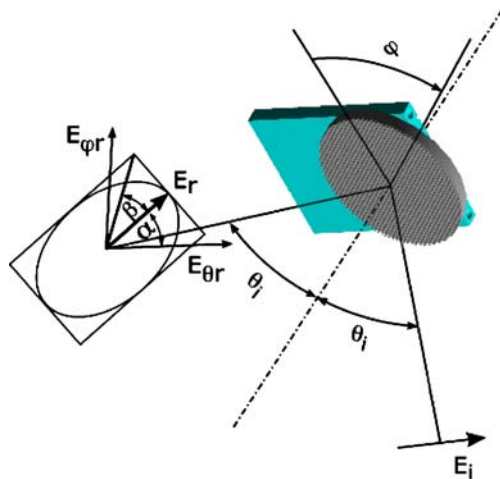
Fig. 6 (a) Field magnitude at parabolic surface (b) normalized coupling coefficient.

A stepwise waveguide cut radiates a cylindrical wave, which illuminates the parabolic mirror surface with an electric field intensity inversely proportional to the squared distance to the reflector surface. A boxcar function is taken for $f_b(y)$ in the plane of beam propagation at the Vlasov converter waveguide aperture as shown in Fig. 5a. Figure 5b shows the maximum field coupling coefficient between the uniform electric field and a Gaussian beam is $c_{ab}^{1y}=0.94$ at $w_{y0}/a=0.505$. The normalized electric field strength at the parabolic mirror surface is

$$f_b(x) = \frac{1}{\sqrt{\pi F \left(1 + \left(\frac{x}{2F}\right)^2\right)}}, \tag{12}$$

which is shown in Fig. 6a. Figure 6b shows that the maximum field coupling coefficient occurs for $c_{ab}^{1x}=0.97$ at $w_{x0}/4F=0.470$. The total power efficiency of the Vlasov converter is found to be 83% by substituting c_{ab}^{1x} and c_{ab}^{1y} into Eq. 11.

Fig. 7 Polarizer geometry.



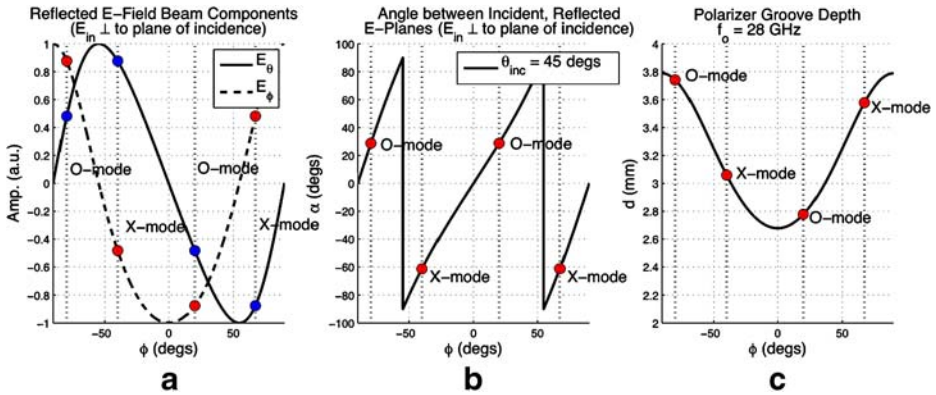


Fig. 8 Polarization rotating twist reflector plate: (a) emergent electric field (b) twist angle (c) groove depth.

Correction of the beam astigmatism and refocusing of the beam is accomplished with two phase-correcting mirrors, M1 (ellipsoidal) and M2 (cylindrical). Dimensions of the mirrors and their curvature radii are large enough that diffraction and truncation losses are small (less than 1% per mirror). Mirror M1 contains an integrated directional coupler consisting of twenty-five 1.2 mm diameter holes machined into the mirror surface along the mirror mid-plane in plane of incidence. The holes, with depths ranging from 1.5 mm to 1.8 mm, couple -35 dB of the incident forward and reflected microwave power to a 6.4 mm by 3.5 mm rectangular waveguide channel machined into the back of the mirror assembly.

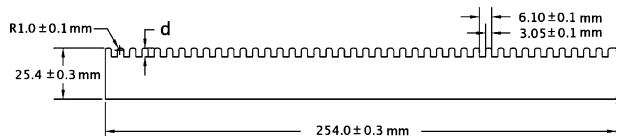
The quasioptical mode converter was designed for the TE_{02} mode and as a result other output modes are inherently filtered by the quasioptical unit due to the variation of θ_B with mode number m, n . All quasioptical components are surrounded by an aluminum enclosure which acts as a biological shield and to ohmically dissipate power from spurious modes.

The electric field of the Gaussian beam must be aligned with or perpendicular to B_0 for O-mode or X-mode heating, respectively. The beam polarization is rotated with a grooved twist reflector plate designed to adjust the phase difference between orthogonal components of the incident electric field [9]. Two X-mode and two O-mode solutions exist for the grooved plate geometry depicted in Figs. 7 and 8. The ECRH transmission line is easily switched between X-mode and O-mode launch by swapping polarizer plates with the appropriate groove depth. The polarizer groove plate profile is shown in Fig. 9, with the X-mode polarizer groove depth $d=3.58$ mm for a rotation angle, $\alpha=67.3^\circ$, and the O-mode depth $d=3.74$ mm for a rotation angle, $\alpha=-79.7^\circ$. Cold testing indicated a cross-polarization less than -25 dB for the X-mode plate and -30 dB for the O-mode plate.

2.2 Dual-mode waveguide

The distance between quasioptical units is traversed by coupling the free space millimeter beam to a smooth, circular cross-section waveguide. The use of the dual-mode waveguide

Fig. 9 Grooved twist reflector plate profile.



effectively solves issues of beam divergence and eliminates the engineering design trade-off between mirror size and mirror quantity existing in quasioptical systems. This waveguide is electrically large (waveguide radius, $a \gg a_{\text{cutoff}}$) to increase alignment tolerances and to reduce the electric field magnitude in the waveguide. A smooth waveguide was chosen over a corrugated waveguide supporting the HE_{11} hybrid mode primarily for cost reduction.

A Gaussian beam will excite an appropriate mixture of the TE_{11} and TM_{11} modes in the circular waveguide. The mode balance constant, B , determines the relative mixture of modes such that the electric field at the waveguide aperture is

$$\mathbf{E}_{ap} = \frac{\mathbf{E}(TE_{11}) + B\mathbf{E}(TM_{11})}{1 + B} \tag{13}$$

The coupling efficiency including a polarization factor is 0.98 at $w_0/r=0.64$ and $B=0.205$. The dual-mode waveguide couples to a Gaussian beam nearly as efficiently as the HE_{11} mode supported in a corrugated waveguide possessing a normalized 2D coupling efficiency of 0.98 with $w_0/a=0.64$ [7, 10].

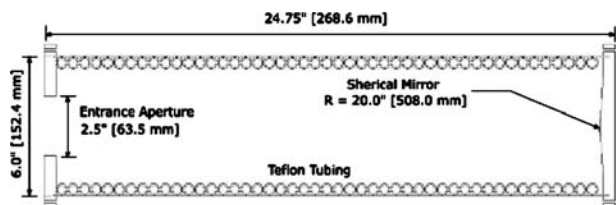
The total length of the dual-mode waveguide must be a multiple of the guided beat wavelength of the two modes in order to achieve efficient coupling to the Gaussian beam at the waveguide exit. The beat wavelength of the TE_{11} and TM_{11} guided wavelengths for a 10.2 cm diameter smooth waveguide is 1.68 m. In this case the total length of the waveguide is 5.04 m, or three beat wavelengths.

2.3 Quasioptical switch and dummy load

A dummy load has been incorporated into the hybrid line to measure the microwave power launched into HSX. The dummy load is located 180 degrees from the corrugated waveguide entrance, which allows the beam to be switched between HSX and the load by rotating an ellipsoidal mirror 90 degrees. The dummy load has an entrance aperture that is the same diameter and distance from the rotatable ellipsoidal mirror pivot point as the corrugated waveguide entrance. This ensures the power delivered to the dummy load is equal to the power launched into HSX.

The dummy load consists of a cylindrical aluminum body, an entrance aperture, a spherical expanding mirror, and a water-carrying teflon tube coiled along the interior length of the body, as shown in Fig. 10. The spherical mirror expands the microwave beam allowing the majority of the power to be absorbed in the water-filled teflon tubes lining the dummy load walls [11, 12]. Real-time water temperature measurements are made between the load entrance and exit with the gyrotron in single pulse mode and/or low duty cycle repetition mode.

Fig. 10 Dummy load cross-section.



2.4 Beam launch assembly

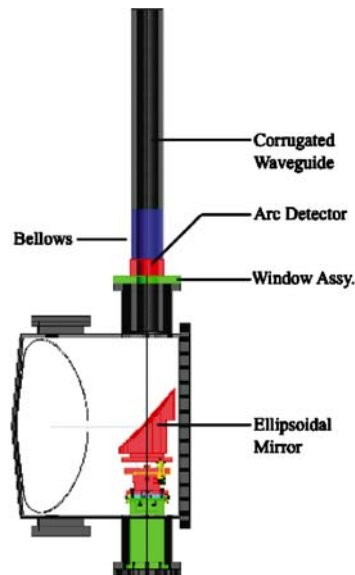
When mirror M3 is switched to HSX, the Gaussian beam is coupled to a 6.35 cm diameter corrugated waveguide and focused in the plasma with ellipsoidal mirror M4 for ECRH plasma breakdown and heating. The corrugated waveguide components, bellows, quartz window assembly and ellipsoidal launching mirror have been retained from the original over-sized waveguide and are shown in Fig. 11. Dry nitrogen is bled into the waveguide at both the gyrotron window and the HSX window to provide convective window cooling and to reduce humidity in the line during operation.

The corrugated waveguide supports the HE_{11} hybrid mode and couples to a free space Gaussian beam in the HSX vacuum vessel. The launching mirror M4 is mounted in the HSX boxport C and is external to the plasma region on the low-field side of HSX. The ellipsoidal mirror focuses the free space Gaussian beam into the HSX plasma region. The beam waist radius at the vacuum magnetic axis is 2 cm, forming a 4 cm diameter spot size.

3 High power testing and plasma operations

High power testing of the hybrid transmission line was performed with the gyrotron microwave source and with the beam line switched to the dummy load. The gyrotron was operated in a low average power testing mode (80–650 W) with a duty cycle of 0.3% (2 ms every 630 ms) as well as in single pulse mode (25–100 kW for 50 ms). Plasma operations have resumed in HSX for 0.5 Tesla X-mode and 1.0 Tesla O-mode ECRH for powers ranging from 25–100 kW.

Fig. 11 HSX ECRH microwave launch system: corrugated waveguide and ellipsoidal mirror.



3.1 Thermal imaging

Imaging of the millimeter beam cross-section was performed by using an infrared thermal camera with a Macor ceramic target. Macor was chosen as a target primarily for its ability to retain a thermal image due to low thermal conductivity. Radiative and convective heat transfer in the ceramic target were neglected, however conduction was found to be non-negligible and a conductive heat transport model was used to model thermal diffusion during the 30 to 60 seconds required to form and capture a thermal image.

A Matlab routine was developed to convert raw infrared images to a temperature map for beam analysis. Thermal measurements reveal a well-formed and symmetric beam at the dual-mode and corrugated waveguide entrances as shown in Figs. 12a, b and 13a, b. Cross-sections of the measured beam waist in and normal to the plane of incidence are shown in Figs. 12c, d and 13c, d and are in good agreement with the predicted shapes when thermal conduction of the pattern is taken into account.

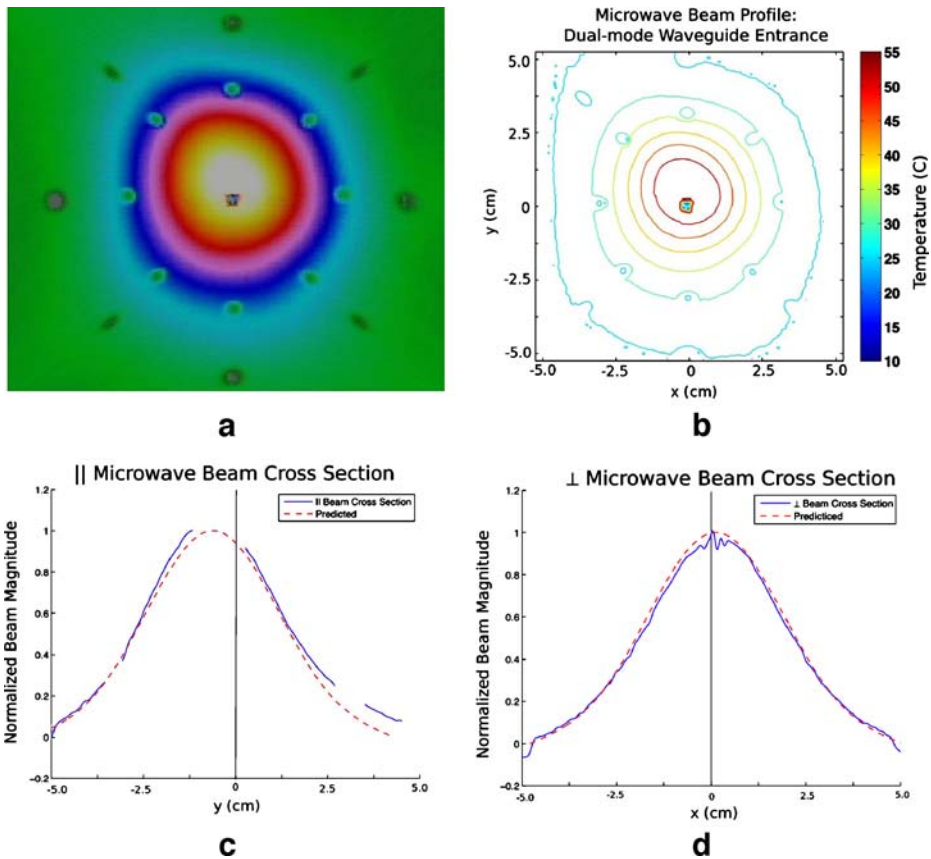


Fig. 12 Dual-mode waveguide entrance: (a) infrared image (b) contour map (c) beam cross section within plane of incidence (d) beam cross section normal to plane of incidence.

3.2 Beam power measurements

The measured launched power for the low average power gyrotron test mode is shown in Fig. 14. The dummy load was calibrated with a 0–700 W variable power heating element to correlate water temperature rise with input microwave power. The input heating power was chosen to correspond to the average power delivered by the gyrotron in the low duty cycle test mode. Instantaneous power output ranging from 25 kW to 100 kW was delivered to the dummy load by varying the gyrotron operating parameters. The measured output power was sensitive to the gyrotron operating regime; optimal measured power was achieved by tuning the gyrotron for maximum output power in the TE_{02} mode.

3.3 ECRH plasma heating

The new transmission has been successfully used for ECRH plasma breakdown and heating for launched power over 100 kW at maximum gyrotron operating parameters. The plasma

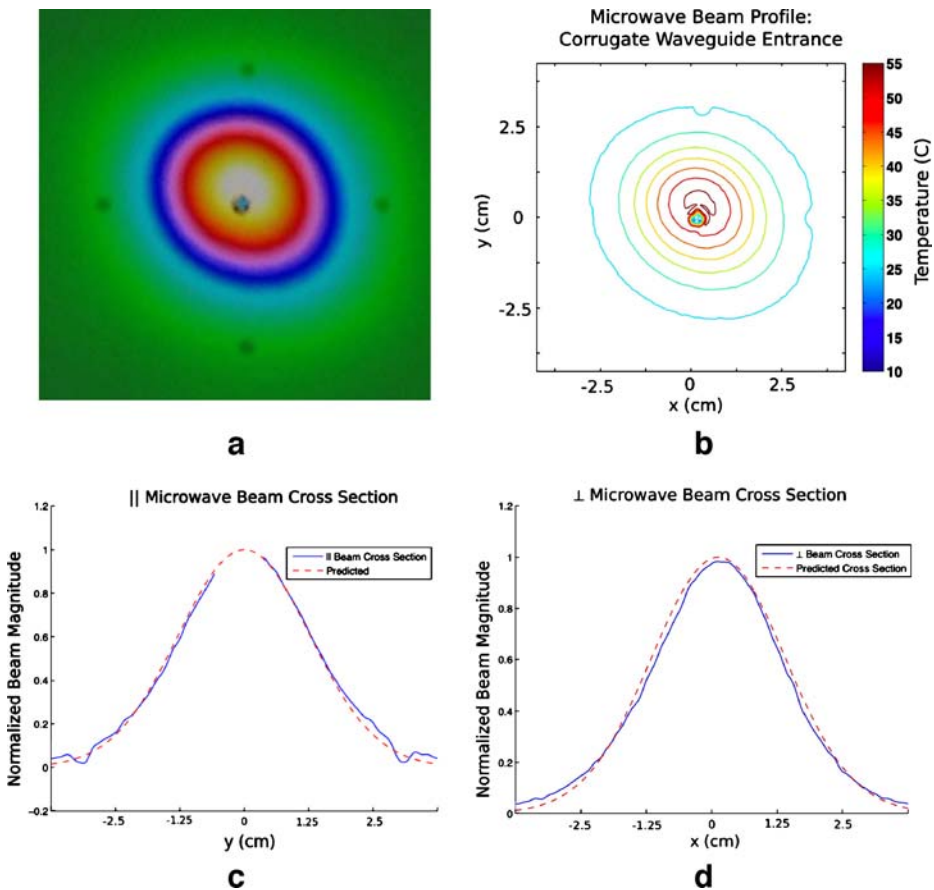
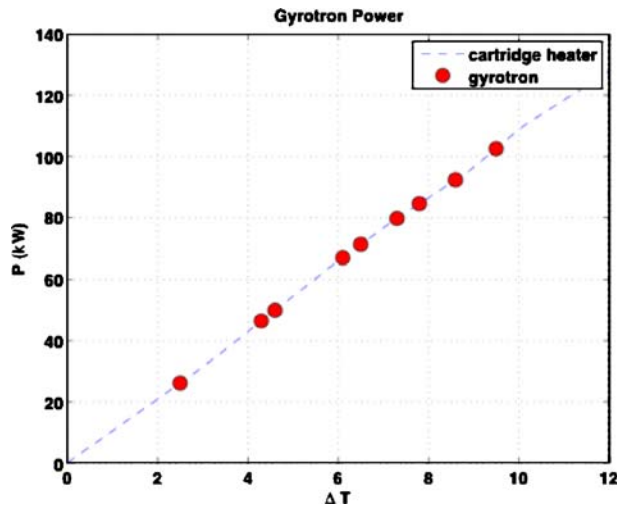


Fig. 13 Corrugated waveguide entrance: (a) infrared image (b) contour map (c) beam cross section within plane of incidence (d) beam cross section normal to plane of incidence.

Fig. 14 Launched power vs. dummy load temperature rise.



stored energy as determined by a diamagnetic flux loop has doubled from approximately 20 Joules with the previous transmission line to approximately 40 Joules with the new hybrid quasioptical line for 50 kW launched power. Improved plasma performance has been attributed to improved mode purity of the beam resulting in higher power density in the heating zone and reduction of power contained in the beam side lobes.

4 Conclusions

A hybrid transmission line has been installed on the HSX stellarator to replace an oversized, mode-converting waveguide. Quasioptical design techniques were employed for mode conversion and manipulation of the beam path. The beam is coupled to a smooth copper waveguide for traversing distances that are a multiple of the TE_{11} and TM_{11} beat wavelength. The waveguide design and component alignment has been verified by thermal image measurements of the microwave beam pattern at two places along the beam path. The line has been successfully tested for launched powers up to 100 kW with an observed increase in plasma stored energy from 20 Joules to 40 Joules for 50 kW launched power. The power level increase has been attributed to the filtering of higher-order modes which results in increased power in the central lobe and reduction of side lobe power levels creating higher power density in the heating region.

References

1. F. S. B. Anderson, A. Almagri, D. T. Anderson, P. G. Mathews, J. N. Talmadge, and J. L. Shohet, *Fusion Technology* **27**, 273 (1995).
2. A. Almagri, D. T. Anderson, P. H. Probert, J. L. Shohet, and J. N. Talmadge, *IEEE Transactions on Plasma Science* **27**, 114 (1999).
3. K. M. Likin, A. Abdou, A. F. Almagri, D. T. Anderson, F. S. B. Anderson, D. Brower, J. Canik, C. Deng, S. P. Gerhardt, W. Guttenfelder *et al.*, *Plasma Physics and Controlled Fusion* **45**, A133 (2003).
4. T. S. Bigelow, T. L. White, and H. D. Kimrey, *Journal of Microwave Power* **21**, 88 (1986).
5. K. Felch, H. Huey, and H. Jory, *Journal of Fusion Energy* **9**, 59 (1990).
6. M. K. Thumm and W. Kasperek, *IEEE Transactions on Plasma Science* **30**, 755 (2002).

7. P. F. Goldsmith, *Quasioptical Systems: Gaussian Beam Quasioptical Propagation and Applications* (Wiley–IEEE Press, New York, 1998).
8. S. N. Vlasov, M. A. Shapiro, and K. M. Likin, *Optics Communications* **88**, 455 (1992).
9. J. D. Hanfling, G. Jerinic, and L. R. Lewis, *IEEE Transactions on Antennas and Propagation* **AP-29**, 622 (1981).
10. P. D. Potter, *Microwave Journal* 71–78 (1963).
11. V. I. Kurbatov, S. A. Malygin, V. B. Orlov, E. A. Solujanova, and E. M. Tai, in *The Fifth International Kharkov Symposium Physics and Engineering of Microwaves, Millimeter, and Submillimeter Waves 2004*, vol. MSMW'04.
12. A. Bruschi, S. Cirant, F. Gandini, G. Granucci, V. Mallera, V. Muzzini, A. Nardone, A. Simonetto, C. Sozzi, and N. Spinicchia, *Nuclear Fusion* **43**, 1513 (2003).